PAPER

Biological Tissue-Equivalent Agar-Based Solid Phantoms and SAR Estimation Using the Thermographic Method in the Range of 3–6 GHz

Teruo ONISHI[†,††a)], **Ryo ISHIDO**[††], ***Members***, **Takuya TAKIMOTO**[††], ***Student Member***, **Kazuyuki SAITO**[†††], **Shinji UEBAYASHI**[†], **Masaharu TAKAHASHI**[†††], ***and*** **Koichi ITO**[†††], ***Members***

SUMMARY In this paper, the electrical constants of a biological tissue-equivalent agar-based solid phantom from 3.0 to 6.0 GHz are described. The developed phantom can reproduce the electrical constants of biological tissues from 3.0 to 6.0 GHz, and it is not necessary to change the phantom for each frequency band in the range of 3.0 to 6.0 GHz during the measurements. Moreover, adjustments to the dielectric constants of the phantom at 3.0, 3.8, 5.2, and 5.8 GHz are presented. The constants of this phantom can be adjusted mainly by using polyethylene powder and sodium chloride. The phantom can be used to evaluate the Specific Absorption Rate (SAR) as well as the antenna characteristics in the range of 3.0 to 6.0 GHz. Furthermore, the effect of the electrical constants of the phantom on the SAR is investigated. The investigation of SAR measurements is performed on the phantom at 5.2 GHz using the thermographic method. Calculations using the FD-TD method and the finite difference method based on the heat conduction equation are carried out in order to evaluate the thermal diffusion in the measurements using the thermographic method. The measured and calculated results are in good agreement. There is evidence that the thermal diffusion influences the SAR estimation at 5.2 GHz more than in a lower frequency range even though this method basically does not depend on the frequency.

key words: *solid phantom, broadband, FDTD method, SAR, thermographic method, heat conduction equation*

1. Introduction

Many studies on measuring and calculating the Specific Absorption Rate (SAR) at frequencies used in mobile phone systems have been conducted [1]–[3]. The SAR is given by

$$\mathrm{SAR} = \frac{\sigma E^2}{\rho} \quad [\mathrm{W/kg}] \tag{1}$$

where σ is the electrical conductivity [S/m], ρ is the density [kg/m^3], and E is the electric field [V/m] (r.m.s.).

Recently, frequencies used by wireless LAN devices that are higher than that used by the present cellular systems have become popular and the Ultra Wide Band (UWB) [4] system, which employs a very wide frequency range, was developed. Since these devices may also be used in close proximity to the human body, investigations on the SAR and antenna characteristics while considering human interaction are very important. Additionally, the International Electrotechnical Commission (IEC) has started to develop a SAR measurement method for which the frequency range is expanded to 30 MHz to 6 GHz [5]. It is expected that this method will be used to test these devices operating at a higher frequency range for SAR compliance.

From these points of view, it is also very important to develop a biological tissue-equivalent phantom that has applicable electrical constants at a point and/or broadband characteristics above 3 GHz. Until now, biological tissue-equivalent liquid and solid phantoms have been proposed in order to evaluate the interaction between the human body and an electromagnetic field at frequencies mostly below 3 GHz [5]–[14]. A few recipes for liquid phantoms for frequencies above 3 GHz have been introduced [5], [9]. Since the E-field probe can be easily scanned in liquid, the liquid phantom has been adopted by the SAR measurement method for compliance, e.g. [8]. On the other hand, the solid phantoms proposed in [11]–[13] have also been used for SAR measurement, which is used to measure the E-field or the temperature rise. One of the features of the solid phantom is that it can maintain an arbitrary shape by itself without a shell.

One of our objectives is the development of a biological tissue-equivalent solid phantom, which has broadband characteristics above 3 GHz. In order to achive this, we focus on a solid phantom based on agar [11], [12], for frequencies above the 3 GHz band. The phantom has been mainly used for dosimetry and evaluating antenna performance in research and development phases. The features of this phantom are its easy adjustment of electrical constants, ease in manufacturing of an arbitrary shape, inexpensive and popular ingredients, and its ability to maintain its shape by itself without a shell. In addition, a heterogeneous phantom can be manufactured.

In this paper, first, adjustments to the electrical constants of the phantom are described from 3 GHz to 5.8 GHz. Then the frequency characteristics of the phantom are described and their broad-band characteristics are presented. In addition, we present the results of a study on the effect of varying the phantom constants.

The investigation of SAR measurement on the solid

Manuscript received September 14, 2004.
Manuscript revised February 28, 2005.

[†]The authors are with NTT DoCoMo, Inc., Yokosuka-shi, 239-8536 Japan.
[††]The authors are with the Graduate School of Science and Technology, Chiba University, Chiba-shi, 263-8522 Japan.
[†††]The authors are with the Research Center for Frontier Medical Engineering, Chiba University, Chiba-shi, 263-8522 Japan.
a) E-mail: oonishite@nttdocomo.co.jp

DOI: 10.1093/ietcom/e88–b.9.3733

phantom using the thermographic method [15] above 3 GHz is performed. A numerical study on the combination between the FD-TD method and the finite difference method based on the heat conduction equation [16] in order to evaluate the effect of thermal diffusion is presented.

2. Solid Phantoms

2.1 Biological Tissue-Equivalent Agar-Based Solid Phantoms

Two kinds of biological tissue-equivalent solid phantoms based on agar have been used to evaluate dosimetry as well as antenna characteristics [11], [12]. One of these phantoms is called the TX-151 phantom [11] and the other is called the Glycerin phantom [12]. Each phantom has different features. Compared to the Glycerin phantom, the TX-151 phantom can simulate high-water content organs such as the brain for a wider frequency range below 3 GHz. On the other hand, the Glycerin phantom can reproduce both high- and low-water content organs and is superior to the TX-151 in terms of preservation. Since the Glycerin provides a moisturizing action, there is less evaporation of water from the Glycerin phantom than that from the TX-151 phantom. Both phantoms can also maintain their shapes by themselves. This means that a container such a shell is not required. Another feature of these phantoms is that arbitrary shapes can be fabricated using a mold.

Figure 1 shows examples of the frequency dependence of the electrical constants of the TX-151 (○) and the Glycerin (△) phantoms with the characteristics of an average brain (●) [17], where the vertical and horizontal axes represent the conductivity and the relative permittivity of the phantoms, respectively. It is obvious that the frequency characteristic ratio of the conductivity to the relative permittivity for the TX-151 phantom is different from that of the Glycerin phantom. This is due to a difference in the ratio of water content between the Glycerin and TX-151 phantoms,

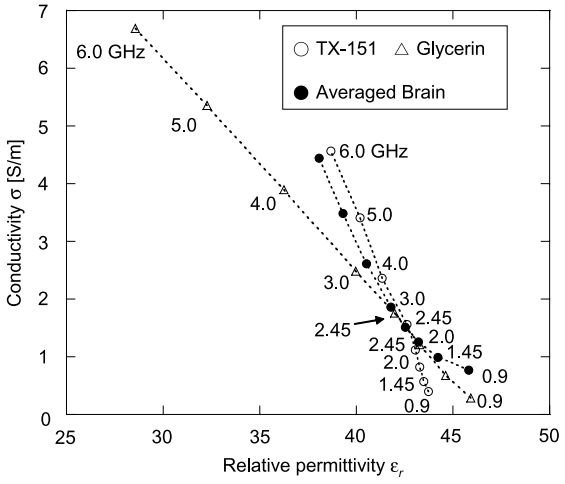

Fig. 1 Examples of frequency dependence of electrical constants of TX-151 and Glycerin phantoms.

e.g. 60% and 80% in total weight. Furthermore, the ratio of glycerin and water in the Glycerin phantom could be another major factor causing the difference. The frequency characteristics of the TX-151 phantom shown in the figure are very similar to those of the average brain especially above 3 GHz without changing the phantom. Therefore, it is anticipated that the TX-151 phantom can be more readily used and easily adjusted to the target value more so than can the Glycerin phantom at frequencies above 3 GHz. Consequently, we will focus from this point on the TX-151 phantom.

2.2 Adjustment of the Electrical Constants of the TX-151 Phantom

The composition of the TX-151 phantom described in [11], [15] as an example is given in Table 1. Agar is used to maintain the shape of the phantom. In order to mix water with the polyethylene powder (PEP), TX-151 is selected for its sticky property. The amount of TX-151 is adjusted according to the amount of PEP [11]. In addition, the conductivity and permittivity of the phantom are mainly dependent on the concentration of NaCl and PEP, respectively.

As mentioned above, the electrical constants of the TX-151 phantom up to 6.0 GHz are experimentally examined. The target electrical constants, an average brain and muscle [17], and head- and body- equivalent phantoms [18] are selected to adjust the TX-151 phantom constants. The head- and body- equivalent phantoms have been used in the SAR measurement procedure with respect to mobile phones in the US [18]. The adjusted electrical constants at 3.0, 3.8, 5.2, and 5.8 GHz are shown in Fig. 2, where the vertical and horizontal axes represent the conductivity and the relative permittivity of the phantoms, respectively. The frequencies of 5.2 GHz and 5.8 GHz are used for wireless LAN systems and the Industrial Scientific and Medical (ISM) band, respectively. The frequency of 3.8 GHz is the center frequency that is the candidate for allocation to future wireless mobile communications. The target values are also plotted as (×) in the figure. We note that the values of the head- and body-equivalent phantoms are only plotted at 3.0 and 5.8 GHz because those at 3.8 and 5.2 GHz are not defined in [18]. The measuring instrument is an HP-85070B dielectric-probe measurement system (Agilent Technology Company, Palo Alto, CA). Each square in the graph represents the electrical constants for each TX-151 phantom, which are changed based on the amount of PEP and NaCl. The vertical and horizontal dotted lines represent the same amount of PEP or NaCl, respectively.

Table 1 Example composition for TX-151 phantom [11], [15].

Ingredient	Amount [g]
Deionized water	3375.0
Agar	104.6
Sodium chloride (NaCl)	21.5
Sodium dehydroacetate	2.0
TX-151	57.1
Polyethylene powder	548.1

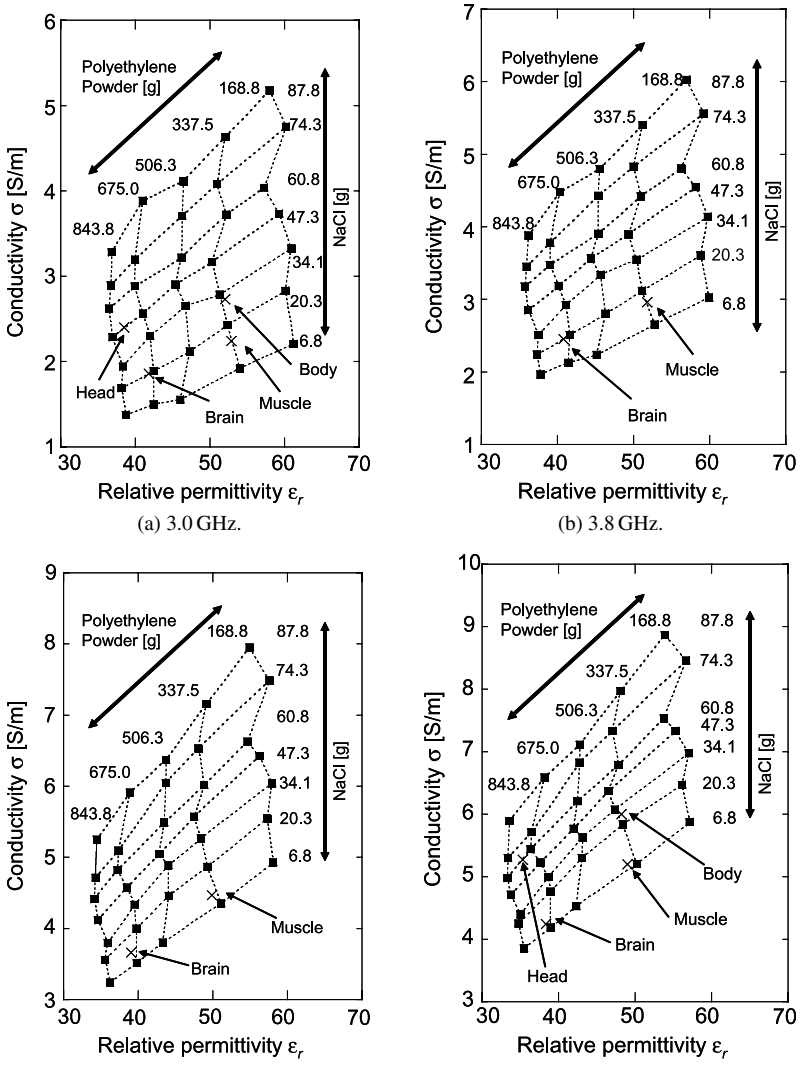

(a) 3.0 GHz. (b) 3.8 GHz.

(c) 5.2 GHz. (d) 5.8 GHz.

Fig. 2 Adjustment of the electrical constants of the TX-151 phantoms.

The amounts of NaCl and PEP are changed to confirm the range of achievable electrical constants of the phantoms. The amounts of other ingredients except for TX-151 are the same as those in Table 1. In Fig. 2, the electrical constants depend on the amounts of both NaCl and PEP. Conductivity depends on the amounts of both NaCl and PEP while the relative permittivity only relies on PEP. Namely, the electrical constants can be controled using the following two-steps procedure. First, the amount of PEP is determined for the desired relative permittivity. For example, 675.0 g of PEP is determined for the brain at 3.0 GHz. Second, the conductivity is adjusted by the amount of NaCl, e.g. 20.3 g of NaCl.

2.3 Electrical Constants versus Frequency

The measured electrical constants of four different types of target values (○), i.e., the average brain, average muscle, and the head- and body- equivalent phantoms, versus the frequency from 3.0 to 6.0 GHz are shown in Fig. 3. We note that the values of the head- and body- equivalent phantoms are only plotted at 3.0 and 5.8 GHz because those at 3.8 and 5.2 GHz are not defined in [18]. The error bars show ±5% of the target values. The amounts of PEP, NaCl, and TX-151 for these four types are shown in Table 2 and the others are the same as described in Table 1. In Fig. 3, the electrical constants of the phantoms are almost within ±5% of the target values at each frequency without changing the composition. This means that by using a unique phantom, a broadband frequency that varies between 3.0 GHz to 6.0 GHz can be covered. Moreover, if the amounts of PEP and NaCl are changed, the phantom can be adjusted to different types of

Table 2 Compositions for TX-151 phantom.

Target	PEP [g]	NaCl [g]	TX-151 [g]
Average brain	675.0	20.3	45.6
Average muscle	337.5	10.0	83.3
Head equivalent	675.0	60.8	45.6
Body equivalent	337.5	34.1	83.3

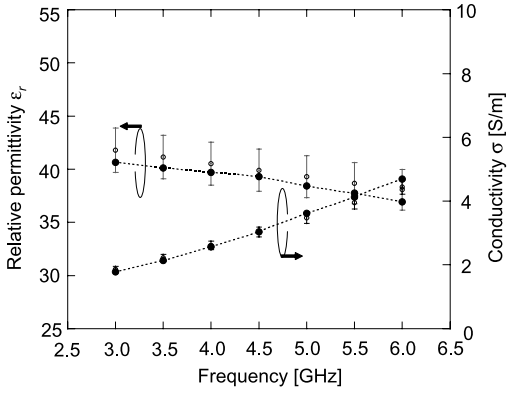

(a) Average brain phantom.

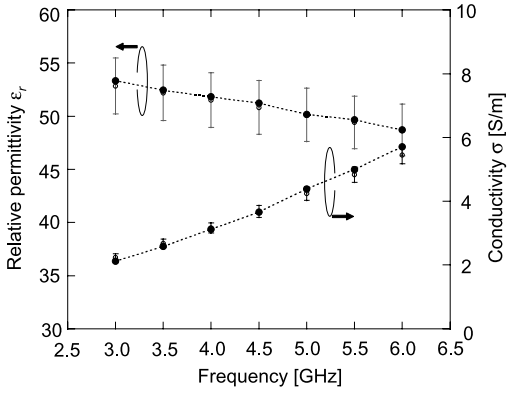

(b) Average muscle phantom.

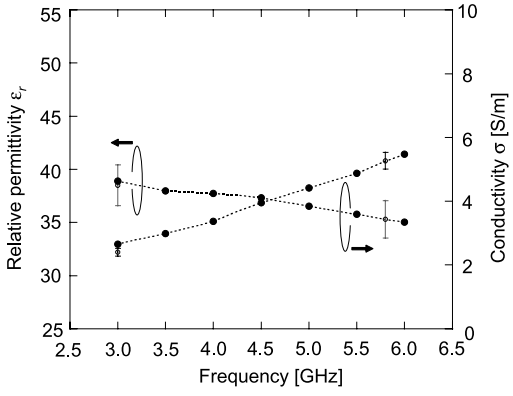

(c) Head equivalent phantom.

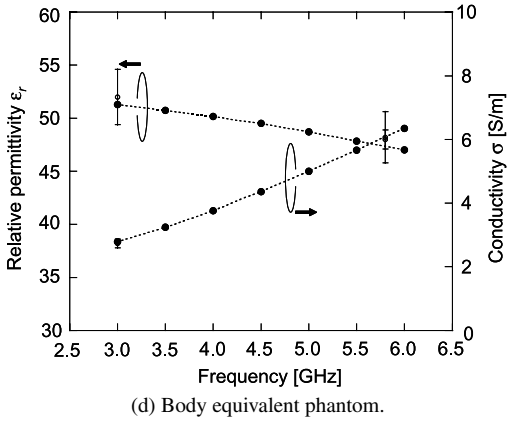

(d) Body equivalent phantom.

Fig. 3 Electrical constants of the TX-151 phantoms versus frequency.

biological tissue.

2.4 Effect of Electrical Constants of the Phantom

The investigation with respect to the effect by variation of the electrical constants for the phantom is important. It is efficient to know the degree to which the variation will impact the SAR before the measurement when a unique phantom is used for a broadband frequency range. In this study, the effect of the variation is estimated using the FD-TD method, assuming a half-wave dipole antenna and a cubic phantom when the relative permittivity and conductivity of the phantom are changed. Similar studies have already been performed [19], [20]. Kawai et al. investigated in detail the effects of the electrical constants of the phantom at 0.9 and 2.0 GHz. Kang et al. [20] also investigated the effect of conductivity in the 2.45 and 5 GHz bands with a change ratio of 75 and 150% compared to the target value described in [18]. In this paper, both the relative permittivity and conductivity are changed and the peak SAR is calculated at 3.8 and 5.2 GHz considering the usage of a unique phantom for the broadband frequency range. The relative permittivity (ϵ_r) and the conductivity (σ) of the phantom at 3.8 GHz and 5.2 GHz are 37.6 and 3.22 S/m, and 36.0 and 4.66 S/m, respectively, which are calculated by a linear interpolation from values taken using a head-equivalent phantom at 3.0 and 5.8 GHz as described by [18].

Table 3 shows the effects of the electrical constants on the peak SAR for both 3.8 and 5.2 GHz. Both the relative permittivity and the conductivity are changed within ±5% because Fig. 3 shows that the electrical constants of each phantom are almost within ±5%. When the relative permittivity is increased, the peak SAR is decreased. On the other hand, when the conductivity is increased, the SAR is also increased. These results are similar to those for 0.9 and 2.0 GHz reported by [19]. However, when the frequency is higher, the effect of the relative permittivity is slightly increased. The worst case variations of the peak SAR at 3.8 and 5.2 GHz are approximately ±6.2% and ±6.6%, respectively, when employing the combination of σ = ±5% and ϵ_r = ∓5%. In this paper, although a more detailed investigation with respect to the SAR measurement procedure, e.g. averaging the SAR, is not performed, variations on the 10g-average SAR are introduced briefly. If the 10g-average SAR is evaluated, the worst case variations at 3.8 and 5.2 GHz are reduced to approximately ±1.0% and ±1.5%, respectively.

Table 3 Effects of electrical constants on peak SAR (Upper: 3.8 GHz, Lower: 5.2 GHz).

$\sigma \setminus \epsilon_r$	-0.95	0	1.05
−0.95	−1.50% −0.98	−3.84 −3.82	−6.10 −6.59
0	2.40 2.90	0 0	−2.30 −2.82
1.05	6.20 6.65	3.74 3.69	1.43 0.81

3. Investigation of SAR Measurement Using the Thermographic Method

3.1 Experimental Configuration

The investigation of SAR measurement on the developed phantom using the thermographic method [15] at 5.2 GHz is performed. Calculations using the FD-TD method and the finite difference method based on the heat conduction equation are carried out to investigate the conditions of the thermographic method. The experimental model is illustrated in Fig. 4. A dipole antenna, the length of which is approximately a half-wavelength, is employed as the source of the electromagnetic energy. The antenna is located 10 mm from the phantom surface. The origin of the model directly faces the antenna feeding point and this point is located on the surface of the phantom. Electrical constants of the phantom are calculated by linear interpolation from values taken using a head-equivalent phantom at 3.0 and 5.8 GHz as described in [18]. In other words, the relative permittivity (ϵ_r) and the conductivity (σ) are 36.0 and 4.66 S/m, respectively. The measurement is performed in a radio anechoic chamber (Graduate School of Science and Technology, Chiba University, Japan). The SAR experimental configuration is shown in Fig. 5. During the measurement, the forwarded power from the power amplifier and the reflected power from the antenna are monitored. The radio anechoic chamber maintains the temperature and humidity, and isolates the experiment from outgoing and incoming radio energy. The phantom is placed far from any air conditioner so that the air from air conditioner did not directly affect the phantom. A TH3102MR thermographic camera (NEC San-ei Instruments Ltd., Japan) is used for the measurement.

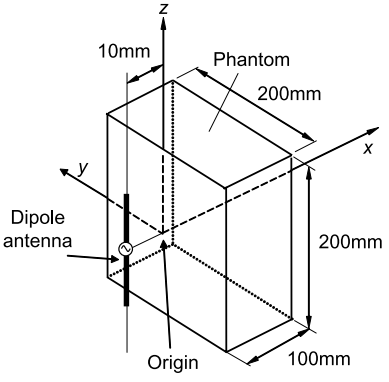

Fig. 4 Experimental model.

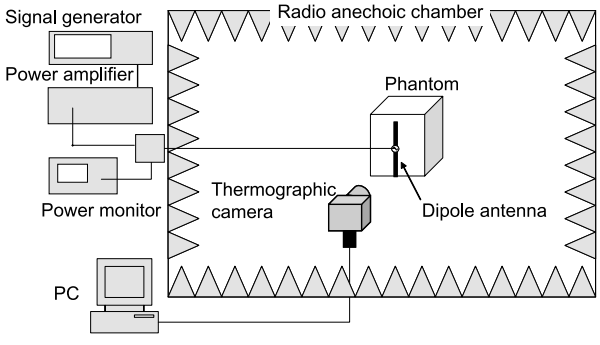

Fig. 5 SAR measurement system.

3.2 Estimation Using the Heat Conduction Equation

When the SAR is measured using the thermographic method, the temperature rise is used directly instead of the electric field shown in Eq. (2).

$$\mathrm{SAR} = c\frac{\Delta T}{\Delta t} \tag{2}$$

where c is the specific heat [J/kg·K] of the phantom material, ΔT is the temperature rise [K] at the point, and Δt is the exposure duration [s]. In this equation, it is assumed that thermal diffusion is negligibly small during the experiment. Consequently, this method is basically independent of the frequency. However, if the frequency is higher such as 5.2 GHz, the SAR distributions will be concentrated in a local area more so than if a frequency below 3 GHz is used. This is because the radiating element is physically smaller and the penetration depth is shallower compared to those at a lower frequency. It is anticipated that the effect of thermal diffusion will be greater. Since in Eq. (2) thermal diffusion is approximated as negligibly small during the experiment, the thermal diffusion can influence the SAR.

In order to investigate the thermal diffusion, the heat conduction equation, Eq. (3), and boundary conditions, Eq. (4) [16], are introduced.

$$\rho c\frac{\partial T}{\partial t} = \kappa\nabla^2 T + \rho\mathrm{SAR} \tag{3}$$

$$-\kappa\left(\frac{\partial T}{\partial n}\right)_n = h(T_\mathrm{S} - T_\mathrm{e}) \tag{4}$$

where κ is the thermal conductivity of the phantom [W/m·K], h is the heat transfer coefficient [W/m^2·K], T_S is the surface temperature, and T_e is the external temperature. In this case, the thermal conductivity (κ) is independent of the location within the phantom. In this study the SAR shown in Eq. (3) is derived from the FD-TD calculation and rise in temperature (ΔT) is evaluated using Eq. (3). The boundary condition, Eq. (4), is adopted at the boundary between the air and the phantom. This condition expresses thermal transfer due to air flow on the surface of the phantom. The finite difference method is used in a numerical calculation for solving Eq. (3) [21]. In the FD-TD method, the cell size in all directions and the time step are 0.5 mm and 0.962 ps, respectively. The Mur's first order absorbing boundary condition is adopted. For the thermal calculation, the cell size and time step are set to 0.5 mm and 0.2 sec, respectively. The cell arrangement in the thermal calculation is the same as that in the FD-TD method. The initial temperature of the phantom is T_e.

Figure 6 shows the calculated SAR distribution along

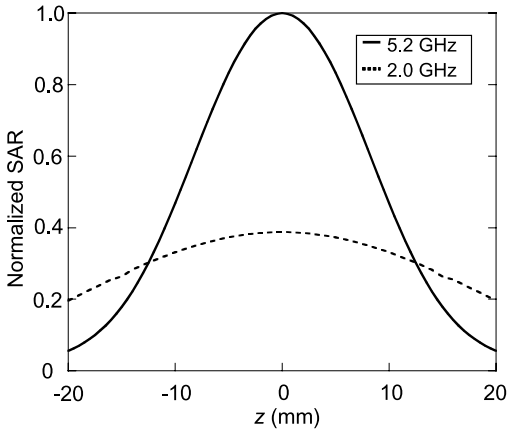

Fig. 6 Normalized SAR distributions along z axis at 2.0 and 5.2 GHz calculated by the FD-TD method.

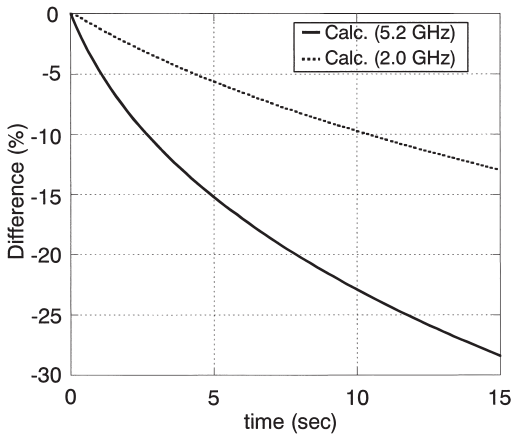

Fig. 8 Calculated temperature rise (ΔT) difference between $h = \kappa = 0$ and $h = 20$ W/m^2·K and $\kappa = 0.5$ W/m·K vs. time.

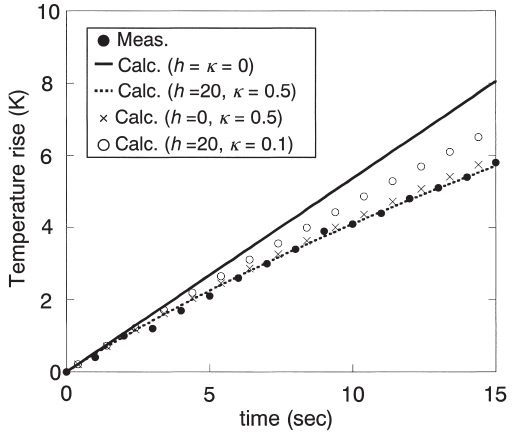

Fig. 7 Calculated and measured temperature rise (ΔT) vs. time at (0.25 mm, 0.25 mm, 0.25 mm).

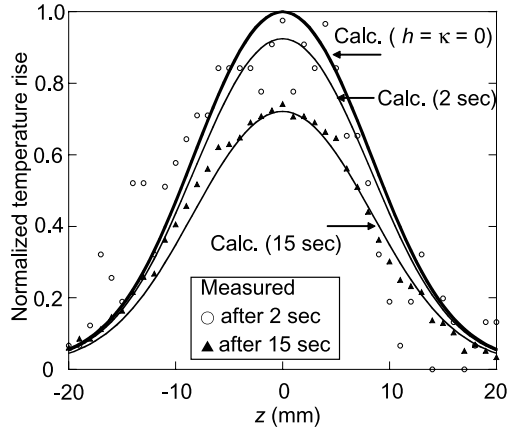

Fig. 9 Normalized temperature rise (ΔT) distributions at 5.2 GHz.

the z-axis at 5.2 GHz. For comparison, the SAR distribution at 2.0 GHz is also plotted. The SAR distributions are normalized to the peak value at 5.2 GHz. It is clear that the SAR distribution at 5.2 GHz is concentrated in a local area more than that at 2.0 GHz.

3.3 Results

The increase in temperature at (0.25 mm, 0.25 mm, 0.25 mm), which is the closest point to the origin, for 5.2 GHz is calculated to estimate the effects of the thermal conductivity (κ) and the heat transfer coefficient (h) (Fig. 7). The thermal conductivity (κ) is 0.5 W/m·K and the heat capacity (c) is 3,700 J/kg·K (measured by Agne Gijutsu Center Co. Ltd., Tokyo, Japan). The heat transfer coefficient (h) is 20.0 W/m^2·K, which is normally used in the estimation, and density (ρ) is 870 kg/m^3. The antenna input power is 9.68 W. In this estimation, the thermal conductivity κ = 0 and 0.1 W/m·K and the heat transfer coefficient $h = 0$ is considered for the comparison. The expression $h = \kappa = 0$ means that no thermal diffusion is considered. As a result, if $h = 20$ W/m^2·K and $\kappa = 0.5$ W/m·K, which is a realistic case, the rise in temperature becomes less prominent compared to $h = \kappa = 0$. In addition, there is no significant change between $h = 0$ and $\kappa = 0.5$ W/m·K. However, the results for h = 20 W/m^2·K and $\kappa = 0.1$ W/m·K exhibit a difference compared to $h = 20$ W/m^2·K and $\kappa = 0.5$ W/m·K. This means that the thermal conductivity inside the phantom influences the temperature rise in this frequency range compared to heat convection from the surface over a short period.

The measured results and those calculated using the heat conduction equation agree fairly well, indicating that the thermal diffusion is well simulated in the calculation. As shown in the figure, both the measured and calculated temperature-rise curves are suppressed when κ is considered and the exposure duration is increased. After approximately 2 sec, the effects of thermal diffusion appear due to thermal conductivity. Figure 8 shows the difference in the temperature increase (%) between $h = \kappa = 0$ and $h = 20$ W/m^2·K and $\kappa = 0.5$ W/m·K at both 2.0 and 5.2 GHz. It appears that temperature increase at 2.0 GHz is suppressed as well. However, the suppression at 5.2 GHz is larger than that at 2.0 GHz as mentioned above.

Figure 9 shows the measured and calculated tempera-

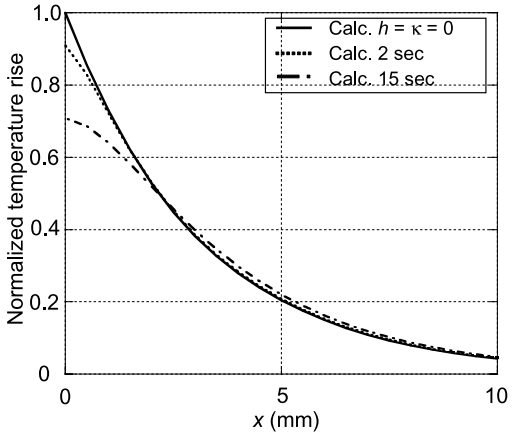

Fig. 10 Calculated normalized temperature rise (ΔT) distributions along x axis.

ture rise distributions along the z-axis at 5.2 GHz for 2 and 15 sec, which are normalized to the calculated maximum temperature rise for $h = \kappa = 0$ for each time, respectively. The measured and calculated temperature rise distributions are in fairly good agreement even though there is variation in the measurement. Figure 10 also shows the calculated temperature rise distributions along the x-axis. As discussed above, when the exposure duration is increased, the temperature rise is lower than that for $h = \kappa = 0$ due to thermal diffusion. It is expected that the estimated SAR from the temperature rise after 2 sec will be mostly within −10%. However, there is a comparatively large variation in the measured values. This is due to the temperature resolution of the thermographic camera used to measure the temperature rise. On the other hand, in the case of 15 sec the estimated SAR is lower than that for 2 sec. The variation in the measurement, however, is smaller because the effect of the resolution is relatively small. As a result, although the thermographic method is independent of the frequency, the exposure duration time must be taken into account in the higher frequency range because the thermal diffusion cannot be neglected. If a thermographic camera with a higher temperature resolution is used and the temperature rise is measured during a very short time such 1 sec, it is possible to derive the SAR without the influence of thermal diffusion.

4. Conclusions

In this paper, the electrical constants of the biological tissue-equivalent agar-based solid phantoms from 3.0 to 6.0 GHz were described. The developed phantoms can reproduce the electrical constants of the biological tissues from 3.0 to 6.0 GHz, and it is not necessary to change the phantom for each frequency band in the range of 3.0 to 6.0 GHz during the measurements. Moreover, the adjustments of the dielectric constants of the phantom at 3.0, 3.8, 5.2, and 5.8 GHz were presented. The constants of this phantom can be adjusted mainly using PEP and NaCl. The phantom can be used to evaluate the SAR as well as the antenna characteristics in the range of 3.0 to 6.0 GHz for research and development in particular.

The effect on the variation of the electrical constants was investigated at 3.8 and 5.2 GHz using the FD-TD method. The maximum variations on the peak SAR at 3.8 and 5.2 GHz were approximately ±6.2% and ±6.6%, respectively, when the combination of $\sigma = \pm 5\%$ and $\epsilon_r = \mp 5\%$ was considered. However, if the SAR is evaluated based on the average volume, i.e., the 10g-average SAR, the worst case variations at 3.8 and 5.2 GHz are reduced to approximately ±1.0% and ±1.5%, respectively. These results can also be applied to the SAR measurement in liquid.

We investigated the SAR measurement at 5.2 GHz using the thermographic method on the developed phantom. Calculations using the FD-TD method and the finite difference method based on the heat conduction equation were carried out in order to evaluate the thermal diffusion in the measurement using the thermographic method. The measured and calculated results were in good agreement. There is evidence that the thermal diffusion influences the SAR estimation at 5.2 GHz more than in a lower frequency range even though this method basically does not depend on the frequency. Therefore, consideration of the influence of the thermal diffusion on the thermographic method at a higher frequency is important.

References

[1] N. Kuster and Q. Balzano, "Energy absorption mechanism by biological bodies in the near field of dipole antennas above 300 MHz," IEEE Trans. Veh. Technol., vol.41, no.1, pp.17–23, Feb. 1992.
[2] M.A. Jensen and Y. Rahmat-Samii, "EM interaction of handset antennas and a human in personal communications," Proc. IEEE, vol.83, no.1, pp.7–17, Jan. 1995.
[3] S. Watanabe, M. Taki, T. Nojima, and O. Fujiwara, "Characteristics of the SAR distributions in a head exposed to electromagnetic fields radiated by a hand-held portable radio," IEEE Trans. Microw. Theory Tech., vol.44, no.10, pp.1874–1883, Oct. 1996.
[4] FCC Part15, "Radio frequency devices," FCC, USA, 2003.
[5] IEC TC106 PT62209 Part2 (draft).
[6] G. Hartsgrove, A. Kraszewski, and A. Surowiec, "Simulated biological materials for electromagnetic radiation absorption studies," Bioelectromagnetics, vol.8, pp.29–36, 1987.
[7] M. Kanda, M. Ballen, C.K. Chou, and Q. Balzano, "Formulation and characterization of tissue simulating liquids used for SAR measurement," Asia-Pacific Radio Science Conference Tokyo, K8-03, p.274, Japan, Aug. 2001.
[8] IEEE Recommended practice for determining the peak spatial-average Specific Absorption Rate (SAR) in the human head from wireless communications devices: measurement techniques, IEEE Standard 1528-2003, 2003.
[9] A.P. Gregory, Y. Johanson, K. Fukunaga, R.N. Clarke, and A.W. Preece, "Traceable dielectric measurements of new liquids for specific absorption rate (SAR) measurement in the frequency range 300 MHz to 6 GHz," Proc. Conference on Precision Electromagnetic Measurements, W2d4, pp.471–472, UK, June 2004.
[10] C.K. Chou, G.W. Chen, A.W. Guy, and K.H. Luk, "Formulas for preparing phantom muscle tissue at various radiofrequencies," Bioelectromagnetics, vol.5, pp.435–441, 1984.
[11] K. Ito, K. Furuya, Y. Okano, and L. Hamada, "Development and the characteristics of a biological tissue-equivalent phantom for microwaves," IEICE Trans. Commun. (Japanese Edition), vol.J81-B-II,

no.12, pp.1126–1135, Dec. 1998.
[12] Y. Okano, K. Ito, and H. Kawai, "Solid phantom composed of glycerin and its application to SAR estimation," IEICE Trans. Commun. (Japanese Edition), vol.J83-B, no.4, pp.534–543, April 2000.
[13] T. Kobayashi, T. Nojima, K. Yamada, and S. Uebayashi, "Dry phantom composed of ceramics and its application to SAR estimation," IEEE Trans. Microw. Theory Tech., vol.41, no.1, pp.136–140, Jan. 1999.
[14] Y. Nikawa, M. Chino, and K. Kikuchi, "Soft and dry phantom modeling material using silicone rubber with carbon fiber," IEEE Trans. Microw. Theory Tech., vol.44, no.10, pp.1949–1953, Oct. 1996.
[15] Y. Okano, K. Ito, I. Ida, and M. Takahashi, "The SAR evaluation method by a combination of thermographic experiments and biological tissue-equivalent phantoms," IEEE Trans. Microw. Theory Tech., vol.48, no.11, pp.2094–2103, Nov. 2000.
[16] P. Bernardi, M. Cavagnaro, S. Pisa, and E. Piuzzi, "SAR distribution and temperature increase in an anatomical model of the human eye exposed to the field radiated by the user antenna in a wireless LAN," IEEE Trans. Microw. Theory Tech., vol.46, no.12, pp.2074–2082, Dec. 1998.
[17] http://www.fcc.gov/fcc-bin/dielec.sh
[18] Federal Communications Commission, "Additional information for evaluating compliance of mobile and portable devices with FCC limits for human exposure to radio frequency emissions," FCC OET Bulletin, no.65 supplement C, edition 01-01, 2001.
[19] H. Kawai, H. Yoshimura, and K. Ito, "Effects of inaccurate electric constants of the tissue-equivalent phantom on the local SAR and the SAR distribution," IEICE Trans. Commun. (Japanese Edition), vol.J85-B, no.5, pp.619–630, May 2002.
[20] G. Kang and O.P. Gandhi, "Effect of dielectric properties on the peak 1- and 10-g SAR for 802.11 a/b/g frequencies 2.45 and 5.15 to 5.85 GHz," IEEE Trans. Electromagn. Compat., vol.46, no.2, pp.268–274, May 2004.
[21] K. Saito, Y. Hayashi, H. Yoshimura, and K. Ito, "Heating characteristics of array applicator composed of two coaxial-slot antennas for microwave coagulation therapy," IEEE Trans. Microw. Theory Tech., vol.48, no.11, pp.1800–1806, Nov. 2000.

Appendix: Consideration of Thermal Diffusion

The effects of thermal conductivity inside the phantom and heat convection from the surface are investigated in this appendix. Figure 7 already indicated that the effect of thermal conductivity inside the phantom is greater than that of heat convection from the surface during a 15 sec period. Equation (A· 1) is called Newton's Law of Cooling, which explains heat convection (the heat flux [W/m^2]) from the surface. This equation is the same as the right part of Eq. (4).

$$q = h(T_{\mathrm{S}} - T_{\mathrm{e}}) \qquad (\mathrm{A}\cdot 1)$$

where q is the heat flux [W/m^2] in terms of the normal direction to the surface, meaning mobility of heat quantity.

In order to estimate the effect of h quantitatively, q is calculated using Eq. (A· 1) at 2 and 15 sec (Table A· 1). In addition, q at 240 sec is calculated for comparison. Since in the thermal calculation the cell size is 0.5 mm, the quantity of heat is obtained by the heat flux × the cell size (0.5 square mm). It is clear that the quantity of heat from the surface increases, as time elapses. On the other hand, the quantity of heat based on the SAR in the volume of 0.5 mm^3, which is independent of time elapse, is 2.16×10^{-4} W. The quantity of heat from the surface is much less than that from the SAR at 2 and 15 sec. However, at 240 sec the quantity of heat from the surface becomes approximately the same as that from the SAR. This indicates that the effect of "h" is not the main role for thermal diffusion during a very short time. In fact, at 240 sec the gradient of thermal distribution normal to the surface is negative though the gradient is positive at 2 and 15 sec (Fig. 10). This means that the direction of heat flux is toward the outside at 240 sec.

Table A· 1 Heat flux from the surface versus time.

	2 sec	15 sec	240 sec
Heat flux [W/m^2]	19.54	114.2	610.6
Quantity of heat [W]	4.89×10^{-6}	2.86×10^{-5}	1.53×10^{-4}

Teruo Onishi was born in Tokyo, in October, 1964. He received his B.S. degree in Physics from the Science University of Tokyo, Japan in 1987. After working for Toyo Communication Equipment Co. Ltd. and Nippon Ericsson K.K., he joined NTT DoCoMo, Inc. He is presently a senior research engineer at the EMC Laboratory, Wireless Laboratories. He is currently attending the Graduate School of Science and Technology, Chiba University, Japan where he is working toward his Ph.D. degree. From 1990 to 1992, he worked in the FD-TD analysis for solving electromagnetic problems with Hokkaido University, Japan. His interests include the standardization of the SAR measurement and the study of EMF, the FD-TD method, antennas for mobile terminals, and printed antennas. He is a member of the IEEE. He is also a member of Technical Group on Human Phantoms for Electromagnetics, IEICE.

Ryo Ishido was born in Aomori, Japan, in August 1979. He received the B.E. degree in electronic communication engineering from Musashi Institute of Technology, Tokyo, Japan, in 2002 and the M.E. degree from Chiba University, Chiba, Japan, in 2004. His main interest is research on the evaluation of the interaction between the electromagnetic fields and the human body.

Takuya Takimoto was born in Chiba, Japan, in April 1981. He received the B.E. degree in urban environmental engineering in Chiba University, Chiba, Japan, in 2004. He is currently working forward the Master degree at the Graduate School of Science and Technology, Chiba University. His research interest is the evaluation of the interaction between the electromagnetic fields and the human body.

Kazuyuki Saito was born in Nagano, Japan, in May 1973. He received the B.E., M.E. and D.E. degrees all in electronic engineering from Chiba University, Chiba, Japan, in 1996, 1998 and 2001, respectively. He is currently a Research Associate at the Research Center for Frontier Medical Engineering, Chiba University. His main interests include the area of medical applications of the microwaves including the interstitial microwave hyperthermia and evaluation of the interaction between electromagnetic fields and the human body. He received an IEICE AP-S Freshman Award, an Award for Young Scientist of URSI General Assembly, an IEEE AP-S Japan Chapter Young Engineer Award, and a Young Researchers' Award of IEICE in 1997, 1999, 2000, and 2004 respectively. Dr. Saito is a member of the IEEE, the Institute of Image Information and Television Engineers of Japan (ITE), and the Japanese Society of Hyperthermic Oncology. He is also a member of Technical Group on Human Phantoms for Electromagnetics, IEICE.

Shinji Uebayashi received the B.E., M.E. and D.E. degrees from Nagoya University, Japan, in 1981, 1983 and 1986, respectively. From 1986 to 1992 he was with NTT Laboratories, Yokosuka, Japan, where he worked on the development of digital cellular system (PDC). Since 1992 he has been with NTT DoCoMo, Inc., where he worked on the development of W-CDMA cellular system and EMC for cellular systems. He is currently the Director of EMC Laboratory in NTT DoCoMo, Inc. His research interests include electromagnetic compatibility and bio-electromagnetics. Dr. Uebayashi is a member of the IEEE, the Institute of Electrical Engineers of Japan (IEE), Japanese Society for Medical Biological Engineering (BME), and of Bioelectromagnetics Society (BEMS).

Masaharu Takahashi received the B.E. degree in electrical engineering in 1989 from Tohoku University, Miyagi, Japan, and the M.E. and D.E. degrees in electrical engineering from Tokyo Institute of Technology, Tokyo, Japan, in 1991 and 1994, respectively. He was a Research Associate from 1994 to 1996, a Assistant Professor from 1996 to 2000 at Musashi Institute of Technology, Tokyo, Japan, and an Associate Professor from 2000 to 2004 at Tokyo University of Agriculture & Technology, Tokyo, Japan. He is currently an Associate Professor at Chiba University, Chiba, Japan. His main interests have been electrically small antennas, planar array antennas (RLSA) and EMC. He received the IEEE AP-S Tokyo chapter young engineer award in 1994. He is a senior member of IEEE.

Koichi Ito was born in Nagoya, Japan, in June 1950. He received the B.S. and M.S. degrees from Chiba University, Chiba, Japan, in 1974 and 1976, respectively, and the D.E. degree from Tokyo Institute of Technology, Tokyo, Japan, in 1985, all in electrical engineering. From 1976 to 1979, he was a Research Associate at Tokyo Institute of Technology. From 1979 to 1989, he was a Research Associate at Chiba University. From 1989 to 1997, he was an Associate Professor at the Department of Electrical and Electronics Engineering, Chiba University, and is currently a Professor at the Research Center for Frontier Medical Engineering as well as at the Faculty of Engineering, Chiba University. He has served as Director of Research Administration Office, Chiba University since April 2005. In 1989, 1994, and 1998, he stayed at the University of Rennes I, France, as an Invited Professor. His main interests include analysis and design of printed antennas and small antennas for mobile communications, research on evaluation of the interaction between electromagnetic fields and the human body by use of numerical and experimental phantoms, and microwave antennas for medical applications such as cancer treatment. Professor Ito is a Fellow of the IEEE, and a member of URSI Commission K in Japan, AAAS, the Institute of Image Information and Television Engineers of Japan (ITE) and the Japanese Society of Hyperthermic Oncology. He served as Chair of Technical Group on Radio and Optical Transmissions of ITE from 1997 to 2001. He also served as Chair of the IEEE AP-S Japan Chapter from 2001 to 2002. He is now Chair of Technical Group on Human Phantoms for Electromagnetics, IEICE, Vice-Chair of the 2007 International Symposium on Antennas and Propagation (ISAP2007) and an Associate Editor of IEEE Transactions on Antennas and Propagation.